Astron. Astrophys. 228, 23–36 (1990)

ASTRONOMY AND ASTROPHYSICS

Star formation history and chemical enrichment in the nuclear regions of M 31 and its dwarf companions M 32 and NGC 205★

E. Bica[1], D. Alloin[2], and A.A. Schmidt[3],★★

[1] Universidade Federal do Rio Grande do Sul, Departamento de Astronomia, Av. Bento Gonçalves, 9500 BR-91500 Porto Alegre-RS, Brazil

[2] Observatoire de Paris, Section de Meudon, Département d'Astrophysique Extragalactique et de Cosmologie, F-92195 Meudon Principal Cédex-France

[3] Universidade Federal de Santa Maria, Departamento de Matematica/NEPAE, Faixa de Camobi, Km 5, BR-97100 Santa Maria-RS, Brazil

Received April 27, accepted July 3, 1989

Abstract. We present a comparative discussion about the stellar population and chemical enrichment in the nuclear regions of M 31 and of its dwarf companions M 32 and NGC 205, from a new set of long slit CCD spectra in the range 3500–10 000 Å. We have performed the population syntheses using a grid of star cluster spectral features as a function of age and metallicity. The algorithm is a multiple minimization procedure, including a statistical treatment of the acceptable solutions and for which we discuss as well the question of the uniqueness of the solution. It provides a more significant result with respect to classical minimization methods relying on a single optimal solution. We find that the semistellar nucleus (SSN) and the bulge of M 31 are dominated by old metal-rich populations. The overall enrichment in heavy elements is however larger in the SSN ($[Z/Z_\odot] \sim 0.6$ at least) than in the inner bulge ($[Z/Z_\odot] = 0.3$). In the visible, flux fractions of 10 to 20% arise from an intermediate age component. The old age components span the entire metallicity range, with a predominant contribution from the highly metallic ones. The young age component remains inconspicuous in the visible range.

In the nucleus of M 32, the metal enrichment comes out to be around solar and the light is dominated by old components in the range $-0.5 < [Z/Z_\odot] < 0$. As much as 30% of the flux at 5870 Å arises from an intermediate age component corresponding to a 15% mass fraction. Both the old metal-poor and the young components in M 32 contribute very little to the visible flux.

Finally, our synthesis shows that the dominant population in the nucleus of NGC 205 is young, in the range 10^8 to $5\,10^8$ yr. The old component with metallicity $-1 < [Z/Z_\odot] < -0.5$ and the intermediate age components provide each around 20% of the visible light. The maximum metallicity attained in this object is $[Z/Z_\odot] = -0.5$.

Key words: galaxies: stellar content of – galaxies: nuclei of – galaxies: evolution of – galaxies: M 31, M 32 and NGC 205

1. Introduction

The stellar content of M 31 and of its dwarf elliptical companions M 32 and NGC 205 has been investigated intensively since Baades's early studies, owing to their apparent brightness.

Population synthesis techniques using a stellar base with colours or spectra have suggested that stars in the nucleus of M 31 are mostly old and metal rich (e.g. Spinrad and Taylor, 1971; Faber, 1972).

The nuclear spectrum of M 32 is less strong-lined and bluer than that of M 31. This might arise from a lower average metallicity and/or from the presence of an important intermediate age component. The various population studies using a stellar base have led, however, to differing conclusions (Spinrad and Taylor, 1971; Faber, 1972; Williams, 1976; O'Connell, 1980, 1986). In particular O'Connell claimed that intense star formation occured at intermediate ages, in this object.

The stellar content of the nucleus in NGC 205 has been mostly studied by means of direct broadband images. It contains luminous blue stars implying recent star formation (Hodge, 1973). Luminous red stars have also been identified which could be evolved stars associated with the young burst of star formation (Gallagher and Mould, 1981). However, part of these red stars turned out to be carbon stars, thus revealing the presence of an intermediate age component (Richer et al., 1984).

An alternative method to study composite stellar populations has been developed, which uses a star cluster spectral library and a grid of the star cluster spectral properties as a function of age and metallicity. (Bica and Alloin, 1986a, 1986b, 1987a). In this synthesis method the IMF and the stellar evolution are implicit in the elements of the base. This simplifies considerably the synthesis problem. The method has provided information on the age and metallicity of the population components in various nuclear spectral types to be found in Shapley-Ames galaxies

Send offprint requests to: D. Alloin

★ Based upon data collected at the Observatoire de Haute Provence (CNRS)

★★ Present address: Astronomy Centre, University of Sussex, Falmer, Brighton BN1 9QH, UK

(Bica, 1988). An advantage of the star cluster method with respect to the stellar synthesis is the fact that the grid of star cluster W_λ (age, $[Z/Z_\odot]$) spans the complete age and metallicity space relevant to the problem. The methods using stellar libraries are restricted to metallicities around solar, in particular for dwarf stars. Then, internal compensations in the synthesis may have distorted the corresponding results. Direct images are important as they can straightforwardly evince certain types of luminous stars associated with a population of a particular age and metallicity. However, as pointed out by Richer et al. (1984), these stars can furnish only crude estimates of the relative proportions of the various population types.

With the hope of getting an improved insight into their nuclear stellar content, we have applied in the present paper the star cluster method to M 31 and companions. We present the observations in Sect. 2 and briefly recall the method in Sect. 3. In Sects. 4, 5 and 6 we present the results for M 31, M 32, and NGC 205 respectively. A search for faint emission lines in the population-subtracted spectra is given in Sect. 7 and the conclusions of this work are summarized in Sect. 8.

2. The observations

The observations were carried out in August 1987 with the Carelec spectrograph at the Cassegrain focus of the 1.93 m telescope at the Haute Provence Observatory. The detector was an 320 vs. 512 RCA CCD array with pixel size 30 μm. The slit width was 3.″5 and the slit length, which was oriented along the East-West direction, spanned the whole chip corresponding to 5.′3 on the sky. Two spectral ranges have been studied, 3500–7300 Å and 6200–10 000Å, with a 150 gr mm^{-1} grating in first order providing a dispersion of 260 Å mm^{-1}. Helium and Argon comparison lamps were employed respectively in the visible and near-infrared regions. The resolution is 18 Å as measured from the FWHM of comparison lines. A Tungsten filament lamp was used for internal flat-fielding after each object frame. With this procedure, the interference fringes in the near-infrared frames could be eliminated through a simple flat-field division. The standard stars BD + 28°4211, Hiltner 102 and G191 B2B were used for flux calibrations (Oke, 1974; Stone, 1977). Typical exposures lasted 5 min for the calibration stars, 10–20 min for M 31 and M 32 and 20–40 min for NGC 205.

The reductions were made with the IHAP and eVe systems at Institut d'Astrophysique de Paris and at Observatoire de Paris/Meudon. A usual procedure for CCD reductions was followed: bias subtraction, flat-fielding correction, spectrum extraction, sky subtraction, wavelength and flux calibrations. Observations of hot standard stars were used for the correction of atmospheric molecular absorptions as described in Bica and Alloin (1987a). Separate sky frames were taken for M 31 whereas for M 32 and NGC 205 the sky was sampled by pixel rows at $1.'4 < r < 2.'6$ away from the nuclei. Pixel rows in the central 8″ were summed up to represent the semistellar nucleus of M 31. The bulge spectrum is the average of regions situated at $5'' \leqslant r < 141''$ on both sides. The spectrum of M 32 corresponds to the high surface brightness central region 54″ long, as there is no prominent semistellar luminosity peak. The pixel rows summed up for NGC 205 correspond to the luminosity peak in the central 11″ diameter region. Adopting $(m - M)_0 = 24.32$ (Sandage and Tammann, 1981) these regions convert into 11 × 26 pc^2(M 31: SSN); 11 × 449 pc^2 centered at $r = 238$ pc (M 31: bulge); 11 × 172 pc^2(M 32); 11 × 34 pc^2(NGC 205). The 900 Å overlapping region of the spectra allowed an accurate merging of the two spectral ranges observed.

Foreground reddening corrections from Burstein and Heiles (1984) were adopted: $E(B - V)_G = 0.08$ for M 31 and M 32; $E(B - V)_G = 0.04$ for NGC 205. We have measured the equivalent widths of strong absorption features with continuum tracing criteria as shown in Bica and Alloin (1988a) and fixed window limits as defined in Bica and Alloin (1986a, 1987a). The W_λ measurements together with the continuum distribution corrected for foreground reddening and normalized to 5870 Å are given in Tables 1a and 1b respectively. They allow to compare the spectral properties of M 31 and companions with those of other galaxy nuclei which we had previously analyzed (Bica and Alloin, 1987a,b).

3. The synthesis algorithm

The population syntheses have been performed with the algorithm described in Schmidt et al. (1989). Since it is a relatively new method we provide below a brief description of the technique employed.

One of the major problems to be faced when synthesizing galaxy spectral properties from a base of simple components such as stars or star clusters is that of non-unique solutions to the mathematical problem one formulates to correlate the basis parameters to the galaxy parameters (spectral features). This results from the presence of intrinsic errors in the observable parameters and the difficulty of building a basis that significantly covers the galaxy features in strength and wavelength. Furthermore, there is always some arbitrariness and particularization of the problem in choosing the representative features, a linear or non-linear function to be minimized and a set of constraints.

Therefore, by nature, the synthesis problem is a degenerate one which has in principle a variety of equally good solutions. From this point of view the frequency of occurence and strength of a given component contribution to the set of acceptable solutions is obviously more significant than the value it may show up in any single optimal solution. Thus a statistical approach should provide a more realistic insight into the problem.

Such a statistical approach has been recently applied to the population synthesis problem by Bica (1988) using a direct combination method which generates and tests possible solutions. This search, however, becomes quite time-consuming and prohibitive to perform for a large number of components. In the present study, we employ a method that combines the power of direct combinations in sweeping the entire solution space with the efficiency of minimization procedures in producing a particular solution. We use the same basis as Bica (1988) which consists of a grid of star cluster spectral features as a function of age and metallicity (Bica and Alloin, 1986a, 1986b, 1987a). This two-parameter basis encloses implicitly the stellar evolution and the IMF as found in Nature, allowing an astrophysical constraint-free formulation of the synthesis problem.

The basis contains 35 components, each being associated with an evolutionary stage of a star cluster at a given metallicity. Each component is represented by a set of six metallic features and three Balmer lines which are not used if some emission contamination is present in the galaxy spectrum. An HII region component is represented by a featureless continuum affected by internal reddening and used independently of the metallicity.

Features of the metal-rich components ($[Z/Z_\odot] = +0.6$) in this basis were extrapolated from lower metallicity values (Bica and Alloin, 1986b). Let us point out that we do not use the full spectral information, having selected the most significant parameters over the range 3500–10 000 Å instead. The function we minimize then is the difference between the equivalent width of the observed features $W_{obs}(i)$ and the synthetic features $W_{syn}(i)$:

$$F(X) = \sum_{i=1}^{9} [W_{obs}(i) - W_{syn}(i, X)]^2 \quad (1)$$

where

$$W_{syn}(i, X) = \sum_{j=1}^{35} X(j)W(i,j)f(i,j) \Big/ \sum_{k=1}^{35} X(k)f(i,k), \quad (2)$$

$$0 \le X(j) \le 1, \quad 1 \le j \le 35, \quad (3)$$

$$\sum_{j=1}^{35} X(j) = 1. \quad (4)$$

$W(i,j)$ is the equivalent width of the i feature of the j component and $f(i,j)$ its corresponding continuum normalized at 5870 Å. The vector X holds the proportions of each component of the basis used to calculate the synthetic features. Expressions (3) and (4) are natural constraints to the components, consistent with Eq. (2).

A minimization procedure is carried out, taking into account the fact that the problem $F(X) \to 0$ has non-unique solutions, i.e., there exists in principle a variety of vectors X that give $F(X) \to 0$ within the observable errors. We compute then a series of minimization tasks for $F(X)$. Each task starts with an initial vector $X = 0$ except for one of its components which is kept at a fixed contribution. The fixed component is then varied by 10% steps between 0 and 100%. Each of the 350 mathematical solutions found, representing a local minimum around the fixed component, is tested against a set of windows of maximum allowed difference between the observed and the synthetic features considered. These windows (see Tables 2, 3, 4 and 6) are chosen in relation to the expected observational errors for each feature. Finally we compute an average solution from the solutions satisfying all feature windows. This average is not only a representative solution, but also each of its components expresses, as a consequence of the statistical approach, its probability of being present in any other acceptable solution, using this basis.

From the analysis of the synthetic features obtained for a sample of galaxy nuclei in Schmidt et al. (1989) we can say that the residuals of an equivalent width normally have a Gaussian distribution within the corresponding window, but not necessarily around the zero value. This can be regarded as resulting from systematic errors in the determination of the equivalent widths due to calibration and continuum tracing uncertainties. The windows of the features we suspect to be subject to such an effect, especially CaIIK, CN 4216 Å and Hδ, are set slightly wider than the expected errors. However, this does not necessarily results in a greater number of solutions to be found since any acceptable solution must satisfy all the feature windows simultaneously.

The degree of degeneracy of the solutions, though heavily dependent on the observable errors, is mainly determined by the internal constitution of the basis with respect to the linear independency of its components and its capacity in describing the evolutionary stage of the object to be modelled. As pointed out in Schmidt et al. (1989), the improvement toward better focused solutions can be achieved more easily by including in the basis additional data over a wider spectral range, mainly in the near-ultraviolet region, than by reducing the observational errors of the features which represents indeed a much more difficult task.

The computations were performed in two ways: one way spans the whole age vs. metallicity plane while the other is restricted to chemical evolutionary paths through this plane. The evolutionary paths can be of two types: in the first one the maximum metallicity is reached within the old age bin and this type is designated by the symbol $A[Z/Z_\odot]$ (e.g. $A[+0.3]$ as in Table 4d); in the second one, designated by $B[Z/Z_\odot]$, an additional metallicity increase is allowed to occur between the old age bin and the $5\,10^9$ yr bin (e.g. $B[+0.3]$ as in Table 4e). The results are expressed in terms of the flux fractions at 5870 Å for each component in the average solution. We also provide the number of acceptable solutions found and the reduced chi-square (χ^2) of the equivalent width residuals for the average solution. The criterium we use to select the best path solutions among all possibilities is based firstly on their resemblance to the whole-plane solution and their correspondence with evolutionary models (Arimoto and Yoshii, 1987), and secondly on their reduced χ^2. Being a parameter basically responsive to global variations of the residuals, the reduced χ^2 is rather dependent on the component variations.

This method of multi-minimization allows to sweep the vector space of solutions generated by the 35 component basis in a fast and efficient way, leading to a representative set of acceptable solutions to the synthesis problem. The code was written in FORTRAN 77 and linked to the MINOS optimization system (Murtagh and Saunders, 1987). The typical CPU time for synthesizing an object was 20 minutes in an ECLIPSE 8000 II computer.

4. M 31: population analysis of the semistellar nucleus and bulge

We compare in Fig. 1 the spectra of the SSN and bulge in M 31 with that of the most strong-lined group for spiral galaxy nuclei, S1, in Bica (1988). Although at first sight these spectra look very similar, measurements for metallic features reveal that the SSN has stronger lines than the bulge, particularly in the windows which are most sensitive to $[Z/Z_\odot]$, such as CN and MgI + MgH (Table 1a). Radial absorption line gradients have also been detected in M 31 by Cohen (1979). However, we point out that separating the observed bulge region into subregions we have found that the W_λ do not vary much throughout the bulge itself. So, at least in the nuclear region considered, there are only two distinct systems: the SSN and the inner bulge. Following Cohen (1979), we find that the near-infrared feature containing the NaI doublet 8183–8195 Å varies strongly (Fig. 1 and Table 1a). However, there is strong evidence that these variations are caused by a molecular feature located slightly redwards of NaI (Alloin and Bica, 1989). In that paper we suggest that the enhancement is simply due to the extremely high metallicity of the SSN and hence, we conclude that the early proposed dwarf-enriched population in galaxy nuclei is no more required.

A detailed comparison of the W_λ for all features shows that S1 has intermediate properties between the SSN and the bulge of M 31. Indeed, group S1 consists mostly of southern Shapley-Ames galaxies, so that for such objects farther away than M 31,

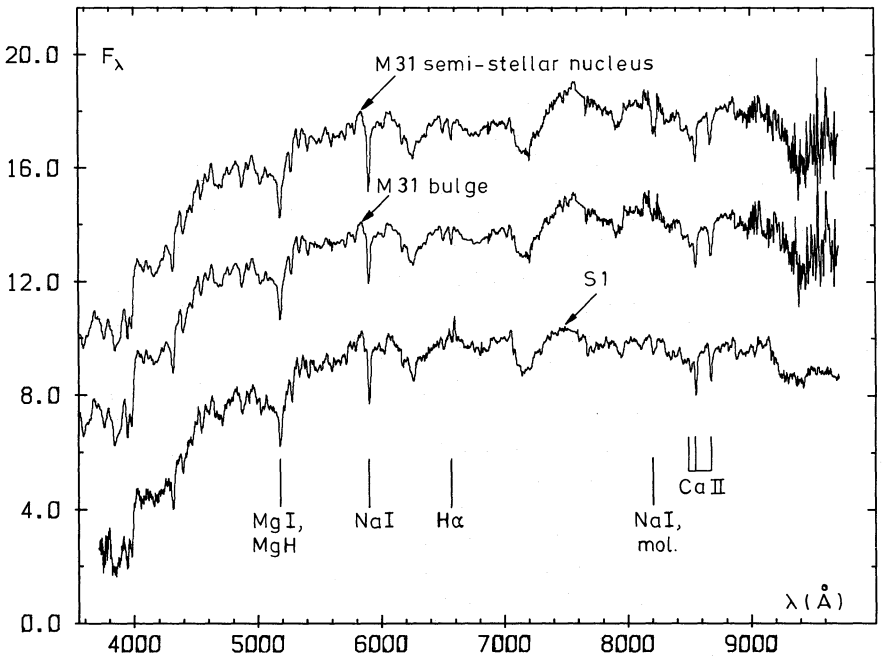

Fig. 1. Comparison of the M 31 nuclear regions, SSN and mean bulge, with the galaxy spectral group S1 (Bica, 1988), consisting of the most strong-lined nuclei within spiral galaxies in our previous studies. All spectra are normalized to $F_\lambda = 10$ at 5870 Å

Table 1a. Measured equivalent widths (Å) for the galaxies. Uncertainties are of 10% for strong absorptions, of 20% for weaker ones ($W < 5$ Å)

Window	Feature identification	Limits (Å)	M 31 (SSN)	M 31 (Bulge)	M 32	NGC 205
2	CN + H9	3814–3862	26.5	23.1	19.5	7.0
3	CN + H8	3862–3908	19.0	16.6	15.3	6.7
4	Ca II K	3908–3952	19.0	17.6	17.5	5.3
5	Ca II H + Hε	3952–3988	13.0	12.5	12.2	10.2
9	Hδ	4082–4124	5.5	4.4	4.3	8.4
10	Fe I	4124–4150	5.6	4.3	3.3	1.9
11	CN	4150–4214	14.4	11.5	8.4	1.3
12	Ca I	4214–4244	5.3	4.7	4.0	1.0
13	Fe I	4244–4284	6.8	6.8	6.0	1.6
14	CH G	4284–4318	9.0	9.2	8.8	3.8
15	Hγ	4318–4364	3.9	4.4	5.2	7.7
16	Fe I	4364–4420	7.3	7.5	7.2	3.0
27	Hβ	4846–4884	3.8	3.2	4.3	6.8
31	Fe I	4998–5064	7.4	6.4	4.9	2.2
32	Fe I, C_2	5064–5130	8.1	7.5	4.8	1.5
33	MgH, C_2	5130–5156	4.2	3.9	2.9	1.0
34	Mg I, MgH	5156–5196	10.1	9.3	7.0	3.1
35	MgH	5196–5244	5.6	5.0	4.4	2.0
36	Fe I	5244–5314	4.6	4.2	4.4	2.5
48	Na I	5880–5914	6.8	5.2	4.5	2.5
54/5/6/7	TiO	6156–6386	22.7	19.2	19.0	11.2
59	Ca I, Fe I	6474–6540	2.0	1.5	1.7	1.7
60	Hα	6540–6586	2.3	1.4	2.8	3.9
62	TiO, [S II]	6670–6736	3.7	3.1	2.9	0.9
66/7/8	TiO	7050–7464	36.0	28.7	27.8	10.7
71	TiO	7704–7852	8.3	9.8	7.5	3.9
72	CN	7852–8040	13.1	13.8	10.5	9.5
74	Na I, TiO?	8160–8234	5.3	2.8	2.2	2.9
75/6	TiO, Ti I	8234–8476	17.4	10.8	14.3	15.0
77	Ca II, TiO	8476–8520	5.8	5.5	5.2	4.4
78	Ca II, TiO	8520–8564	7.2	6.8	6.8	5.7
79	P14, TiO	8564–8640	5.7	5.7	4.5	3.2
80	Ca II, TiO	8640–8700	6.3	6.4	5.5	5.5
81	P12, Fe I	8700–8786	3.4	2.2	2.2	2.4
83/4	TiO, P11 + 10	8844–9066	11.1	7.6	8.4	5.6

Table 1b. Continuum points F_λ relative to F_λ (5870 Å) corrected for the foreground reddening (Sect. 2)

λ (Å)	M 31 (SSN)	M 31 (Bulge)	M 32	NGC 205
4020	0.48	0.55	0.58	1.04
4570	0.79	0.84	0.86	1.07
5340	0.94	0.96	0.95	1.02
6630	0.99	0.99	0.93	0.88
6990	0.99	0.99	0.93	0.85
7520	1.08	1.08	0.97	0.83
8040	1.06	1.08	0.94	0.80
8408	1.06	1.07	0.92	0.75
8700	1.06	1.05	0.91	0.72
9100	1.05	1.04	0.90	0.68

we are observing through the spectrograph slit a *mixture* of nuclear subsystems like those encountered in M 31: SSN and inner bulge.

We show in Table 2a the whole-plane synthesis results for the M 31 SSN. The dominant population is the old metal rich component at $[Z/Z_\odot] = 0.6$. There is a steeply increasing contribution towards high metallicities in the old age bin and smaller contributions from intermediate ages. Notice also that the young component remains almost inconspicuous in the visible and near-infrared ranges. Else, it is known that the nucleus in M 31 exhibits an upturn in the ultraviolet (e.g. Welch, 1982). We have recently analyzed the spectra of giant elliptical galaxies from 1200 to 9700 Å using a modified version of the star cluster method (Bica and Alloin, 1988b). We have concluded that recent star formation at a small rate or a hot component associated with the old metal-rich component can explain the upturn. In particular we have excluded the possibility that the upturn is caused by a

Table 2. Flux fractions (%) at 5870 Å for various models and comparison to observations (test), for the SSN in M 31. (a) the whole-plane solution; (b) the path solution of type *A*, up to $[Z/Z_\odot] = 0.6$, labelled *A*[0.6]

RH II	E7	5 E7	E8	5 E8	E9	5 E9	>E10	Age $[Z/Z_\odot]$
Table 2a								
0	1.0	0	0	0.1	1.5	14.4	54.4	+0.6
				0.1	0.4	7.3	9.3	+0.3
				0.1	0.4	2.8	2.8	0.0
				0.8	0.1	0.8	2.2	−0.5
					0.1	0.4	0.4	−1.0
						0.1	0.1	−1.5
							0.1	−2.0
Acceptable solutions: 75; $\chi^2 = 0.623$								
Table 2b								
0	1.6	0	0	0.3	3.8	19.3	49.4	+0.6
							15.5	+0.3
							4.8	0.0
							4.0	−0.5
							0.7	−1.0
							0.2	−1.5
							0.2	−2.0
Acceptable solutions: 44; $\chi^2 = 0.638$								

Test

Features	Observed W_λ (Å)	Window (Å)	Residue (Å)	
			a	b
Ca II K	19.0	2.5	0.7	0.7
CN 4216	14.4	3.0	−0.3	−0.5
CH G band	9.0	1.5	−0.9	−1.0
Mg I + MgH	10.1	1.8	0.8	0.8
Ca II 8542	7.2	1.2	0.7	0.7
Ca II 8662	6.3	1.2	0.5	0.5
Hδ	5.5	2.5	0.4	0.5
Hγ	3.9	2.0	−1.4	−1.3
Hβ	3.8	1.2	−0.3	−0.2

hot component associated with the small amount of old metal-poor components. Owing to the similarity of the spectra of the M 31 nucleus with those of giant elliptical galaxies, the situation might be basically the same. A detailed analysis of this point would require however the completion of the star cluster spectra library in the range 3000–3700 Å and their linking with UV data from IUE, between 1200 and 3000 Å.

The path solution with best χ^2 is $A[0.6]$ (Table 2b): it resembles very much the whole-plane solution. These results are very close to those obtained for groups S1 and E1, the strong-lined nuclei in spiral and elliptical galaxies (Bica, 1988). It is worth noticing that the whole-plane solution for M 31 SSN, which was derived without astrophysical constraints, yields a result which is compatible with chemical evolution theoretical predictions, as in the synthesis for group E1 (Schmidt et al., 1989).

Results for the M 31 bulge are shown in Table 3. The whole-plane solution comes out rather complex, a case already faced with group S3 in Schmidt et al. (1989). Although a complicated scenario in terms of merging between metal-poor and metal-rich populations could be figured out, this is quite unprobable for the present case. We interpret this result rather as an artefact due to internal compensations in the method which lead to a mathematically better solution with less astrophysical meaning. A wider spectral coverage may give, in the future an astrophysically more plausible whole-plane solution. For the moment the best approach is to restrict the synthesis to chemical evolutionary paths. The best χ^2 is then obtained for model $A[0.6]$, which still resembles the whole-plane solution. The next better χ^2 is for $A[0.3]$ (Table 3b), which gives a steeply increasing contribution in the old age bin. The path $B[0.6]$ which differs from $A[0.3]$ in having an increase in $[Z/Z_\odot]$ from 0.3 to 0.6 dex between the old age and the intermediate age bins, presents similar χ^2 and flux fractions. These results indicate that the dominant population is old and metal-rich ($[Z/Z_\odot] = 0.3$) with a 10% flux con-

Table 3. Same as Table 2 for the bulge in M 31. (a) the whole-plane solution; (b) the path solution of type A, up to $[Z/Z_\odot] = 0.3$, labelled $A[0.3]$

RH II	E7	5 E7	E8	5 E8	E9	5 E9	> E10	Age $[Z/Z_\odot]$
Table 3a								
0.5	0.8	0	0	0.1	0.4	6.4	48.4	+0.6
				0.1	0.4	3.5	8.5	+0.3
				0.1	0.1	2.7	4.8	0.0
				0.2	0.1	1.5	18.0	−0.5
					0.1	0.8	1.4	−1.0
						0.4	0.4	−1.5
							0.5	−2.0
Acceptable solutions: 79; $\chi^2 = 0.743$								
Table 3b								
0.4								+0.6
	1.3	0	0	0.4	1.1	10.6	64.0	+0.3
							15.1	0.0
							5.9	−0.5
							0.5	−1.0
							0.4	−1.5
							0.4	−2.0
Acceptable solutions: 28; $\chi^2 = 0.810$								

Test

Features	Observed W_λ (Å)	Window (Å)	Residue (Å)	
			a	b
Ca II K	17.6	2.5	0.9	0.8
CN 4216	11.5	3.0	−1.3	−1.3
CH G band	9.2	1.5	−0.1	−0.2
Mg I + MgH	9.3	1.8	1.0	1.2
Ca II 8542	6.8	1.2	0.7	0.9
Ca II 8662	6.4	1.2	1.0	1.1
Hδ	4.4	2.5	−0.3	−0.2
Hγ	4.4	2.0	−0.7	−0.6
Hβ	3.2	1.2	−0.6	−0.5

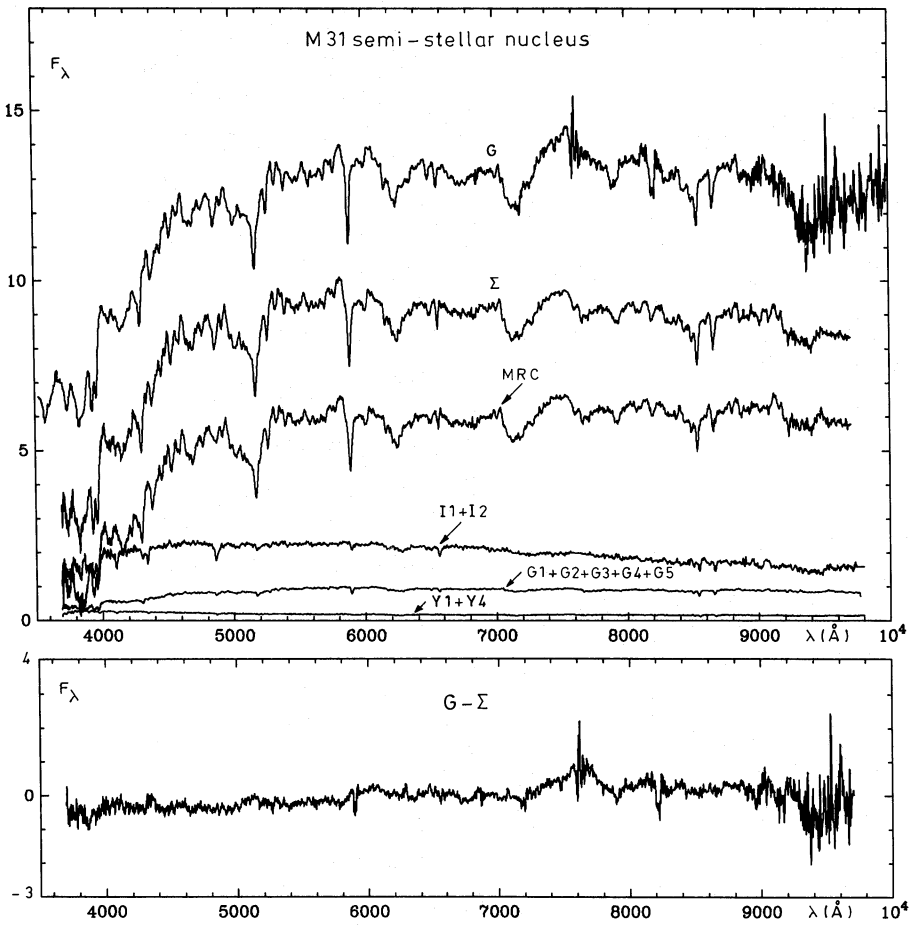

Fig. 2. Visualization of the grid synthesis solution $A[0.6]$ for the M 31 SSN, using the real star cluster spectral groups for metallicities up to $[Z/Z_\odot] = 0$ and the "predicted" star cluster for $[Z/Z_\odot] = 0.6$ (Bica, 1988). The latter spectrum labelled metal rich cluster (MCR) in the figure, stands for the fractions, within the old age bin, at $[Z/Z_\odot] =$ 0.6 and 0.3. For details see Table 2b. The real galaxy spectrum has been corrected for the foreground reddening $E(B-V)_G = 0.08$ and an internal reddening $E(B-V)_i = 0.07$. For clarity, the galaxy spectrum G has been shifted along the vertical axis. Residuals galaxy minus synthesis (G − ∑) are displayed in the lower set

tribution at 5870 Å from intermediate ages. The old metal-poor and young components are negligible.

We emphasize that the computations with the multi-minimization algorithm are carried out with a star cluster grid of W_λ covering wide ranges in age and metallicity. The visualization of the results provided in Figs. 2 to 5 is given in terms of the *available* star cluster groups of spectra as close as possible to the grid solutions (Bica, 1988; see also Table 7 for the properties of star cluster spectra). Visualization of the synthesis results for the SSN of M 31 (Table 2b) is displayed in Fig. 2. Owing to the extremely high metallicity in this object, we have used in addition to real cluster spectra available within the base, the extrapolated cluster spectrum predicted by Bica (1988) for old ages at $[Z/Z_\odot] = 0.6$. An internal reddening $E(B-V)_i = 0.07$ is needed for the spectral energy distribution of the M 31 SSN to match the synthetic spectrum (after the foreground reddening correction $E(B-V)_G =$ 0.08 has been applied). For the bulge of M 31, the visualization in terms of real star cluster spectra for path $A[0.3]$ is presented in Fig. 3. Particularly important for the visualization of the synthesis of red strong-lined galaxy nuclei reaching up a metallicity not higher than $[Z/Z_\odot] = 0.3$ is the globular cluster group G1, which contains clusters like NGC 6528, much more strong-lined than globular clusters usually called metal-rich in the literature like 47 TUC. The real bulge spectrum previously corrected for foreground reddening $E(B-V)_G = 0.08$ requires an additional internal reddening $E(B-V)_i = 0.05$ to match the synthetic spectrum.

We conclude that the SSN and the bulge of M 31 are dominated by the old metal-rich components, and that the metallicity is higher in the SSN.

5. The nucleus of M 32

We show in Table 4 results of the synthesis for M 32. As for the M 31 bulge, the whole-plane solution for M 32 (Table 4a) is quite complex suggesting mathematical internal compensations. We thus proceed to chemical evolutionary path solutions. The best χ^2 occurs for model $A[0.0]$ (Table 4b). Alternative solutions are $B[0.0]$, $A[0.3]$ and $B[0.3]$ respectively provided in Tables 4c to 4e. The resulting continuum points are compared with observations in Table 5. The second column is the observed spectrum corrected for the foreground reddening $E(B-V)_G = 0.08$. The third column has an additional correction assigned to internal reddening $E(B-V)_i = 0.05$. The best model in terms of absorption features, $A[0.0]$ is also the best one in terms of continuum distribution. Model $B[0.0]$ has a larger χ^2 and is excessively blue. Models $A[0.3]$ and $B[0.3]$ have a reasonable continuum, but their χ^2 is worse than in $A[0.0]$. Furthermore the flux fractions for path $A[0.3]$ are rather complex, with a maximum in the middle of the old age bin. Low metallicity paths like $A[-0.5]$

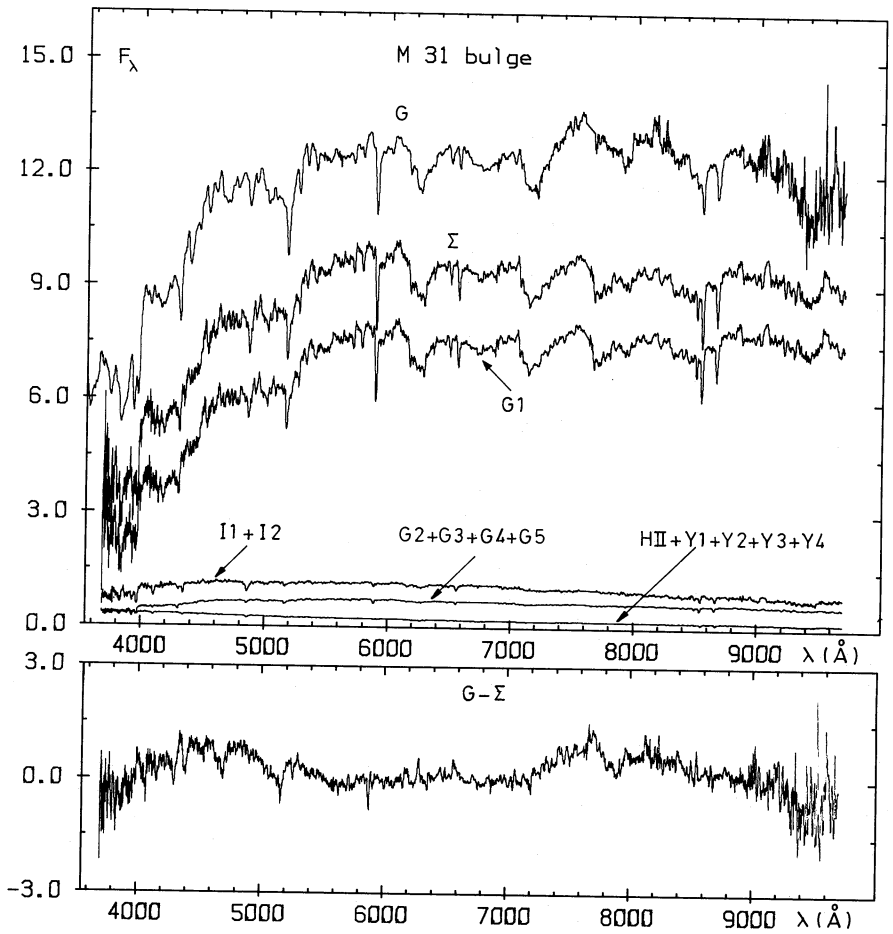

Fig. 3. Visualization of the grid synthesis solution $A[0.3]$ for the M 31 bulge ($\sum$) using only the real star cluster spectral groups (Gi, Ii, Yi) available. The old age bin components for $[Z/Z_\odot] = 0.3$ and 0 are both represented by the star cluster group G1. For the age and metallicity values of these groups see Table 7. This is why the "apparent" residues are larger. The real galaxy spectrum is reddening corrected: foreground $E(B-V)_G = 0.08$ and internal $E(B-V)_i = 0.05$. For clarity the observed spectrum G has been shifted along the vertical axis

Table 4. Same as Table 2 for the central region in M 32, (a) the whole-plane solution; (b) the path solution of type A, up to solar metallicity labelled $A[0.0]$; (c) the path solution of type B, up to solar metallicity labelled $B[0.0]$.; (d) the path solution of type A, up to $[Z/Z_\odot] = 0.3$ labelled $A[0.3]$; (e) the path solution of type B, up to $[Z/Z_\odot] = 0.3$ labelled $B[0.3]$

RH II	E7	5 E7	E8	5 E8	E9	5 E9	>E10	Age $[Z/Z_\odot]$
Table 4a								
0	0	0	0	0.1	0.6	14.0	13.4	+0.6
	0	0	0	0.1	0.6	2.8	3.7	+0.3
	0	0	0	0.1	0.6	5.5	5.8	0.0
	0	0	0	0.2	0.6	9.4	34.6	−0.5
					0.6	2.3	3.0	−1.0
						0.6	1.2	−1.5
							0.3	−2.0
Acceptable solutions: 100; $\chi^2 = 1.328$								
Table 4b								
0								+0.6
								+0.3
	0	0	0	0.3	1.8	29.6	41.2	0.0
							24.2	−0.5
							2.2	−1.0
							0.3	−1.5
							0.3	−2.0
Acceptable solutions: 33; $\chi^2 = 1.254$								

RH II	E7	5 E7	E8	5 E8	E9	5 E9	>E10	Age $[Z/Z_\odot]$
Table 4c								
0								+0.6
								+0.3
	0	0	0	0.5	1.5	69.7		0.0
							24.7	−0.5
							2.6	−1.0
							0.5	1.5
							0.5	−2.0
Acceptable solutions: 20; $\chi^2 = 1.353$								
Table 4d								
0								+0.6
	0	0	0	0.2	1.4	20.9	14.4	+0.3
							18.1	0.0
							37.1	−0.5
							5.7	−1.0
							1.4	−1.5
							0.7	−2.0
Acceptable solutions: 44; $\chi^2 = 1.299$								
Table 4e								
0								+0.6
	0	0	0	0.3	1.7	25.4		+0.3
							31.9	0.0
							32.8	−0.5
							5.4	−1.0
							1.7	−1.5
							0.8	−2.0
Acceptable solutions: 37; $\chi^2 = 1.326$								

Test

Features	Observed W_λ (Å)	Window (Å)	Residue (Å)				
			a	b	c	d	e
Ca II K	17.5	2.5	1.8	1.7	1.8	1.7	1.7
CN 4216	8.4	3.0	−2.0	−1.9	−1.8	−2.0	−2.0
CH G band	8.8	1.5	0.3	0.3	0.4	0.3	0.3
Mg I + MgH	7.0	1.8	0.1	0.3	0.5	0.2	0.3
Ca II 8542	6.8	2.0	1.5	1.6	1.6	1.6	1.6
Ca II 8662	5.5	2.0	0.7	0.7	0.8	0.7	0.8
Hδ	4.3	2.5	−0.7	−0.5	−0.7	−0.4	−0.5
Hγ	5.2	2.0	−0.2	−0.1	−0.4	0.0	0.0
Hβ	4.3	1.2	0.1	0.2	−0.3	0.4	0.3

have been rejected by the algorithm owing to prohibitive residuals. In fact the nucleus of M 32 is far too strong-lined for paths at $[Z/Z_\odot] = -0.5$.

We conclude that the best synthesis result is indeed that corresponding to model $A[0.0]$, which is visualized in Fig. 4. It indicates that the nucleus of M 32 has reached up the solar metallicity. The intermediate age component represents an important flux fraction at 5870 Å (≈30%), but it is not dominant. According to the M/L_v dependence on age for a single generation system (Bica et al., 1988), this corresponds to ≈11% in mass fraction. The old components are dominant with flux fractions of 41% at $[Z/Z_\odot] = 0$ and 24% at $[Z/Z_\odot] = -0.5$. The old metal-poor components ($[Z/Z_\odot] \leq -1$) and the young age components can be neglected.

We thus find evidence that the nucleus of M 32 is composite in age and metallicity. Oversimplifications in particular of its metallicity, might explain some of the conflicting results from previous stellar syntheses (Sect. 1).

Table 5. Real and synthetic continuum distributions, F_λ/F_λ (5870 Å), for M 32

λ (Å)	Observed		Synthetic			
			A[0.0]	B[0.0]	A[0.3]	B[0.3]
4020	0.58	0.62	0.66	0.78	0.64	0.66
4570	0.86	0.90	0.85	0.92	0.84	0.85
7520	0.97	0.94	0.93	0.91	0.93	0.93
8700	0.91	0.87	0.91	0.87	0.91	0.90

Notes: Column 2 is the observed spectrum corrected for the foreground reddening $(E(B-V)_G = 0.08$; column 3 is column 2 corrected for internal reddening $E(B-V)_i = 0.05$, in addition.

6. The nucleus of NGC 205

Table 6 provides results of the synthesis for the nucleus in NGC 205. The whole-plane solution is shown in Table 6a. NGC 205 is a blue nucleus and the solution tends to scatter over the age vs. metallicity plane. This is certainly due to the limited information contained in the visible and near-infrared spectral ranges when nuclei dominated by relatively hot blue components are to be synthesized. However, the whole-plane solution tells us that the dominant component is $\approx 5\,10^8$ yr old and is metal deficient. The chemical evolutionary path solution with best χ^2 is $A[-0.5]$ (Table 6b). It indicates again that the $5\,10^8$ yr old and the other blue components are dominant. We find flux contributions of about 20% from intermediate ages and of 10% from the old age bin which presents increasing contributions towards $[Z/Z_\odot] = -0.5$. The path $B[-0.5]$ has very similar χ^2 and component contributions. Paths attaining the solar metallicity have χ^2 larger by 25%, of which we show B[0.0] in Table 6c. The basic difference with respect to Table 6b is the transfer of part of the intermediate age components towards younger ages and towards the old age bin. The dominant population migrates from $5\,10^8$ to 10^8 yr. The solutions reaching $[Z/Z_\odot] \geq 0.3$ have larger χ^2 and show a complex behaviour in the old age bin: consequently they have been discarded.

Although the previous computations have strongly suggested model $A[-0.5]$ as providing the best results, we have performed additional tests in the case of NGC 205. So far in the calculation we have used the W_λ from the grid of star cluster spectral properties and the associated line continua. As the synthetic W_λ depend only to the second order on the line continuum, this method does not fully use the information contained in the spectral energy distribution. Thus we now perform an additional synthesis using the point to point spectrum of NGC 205 in the range 3700–9700 Å with a 2 Å step. The base consists of the star cluster spectral groups of Bica (1988), which have been used for the visualizations of grid synthesis results in Sects. 4 and 5. The metallicity of these groups for ages $t \leq 5\,10^9$ yr are particularly suitable for a spectral synthesis of NGC 205, as the star clusters

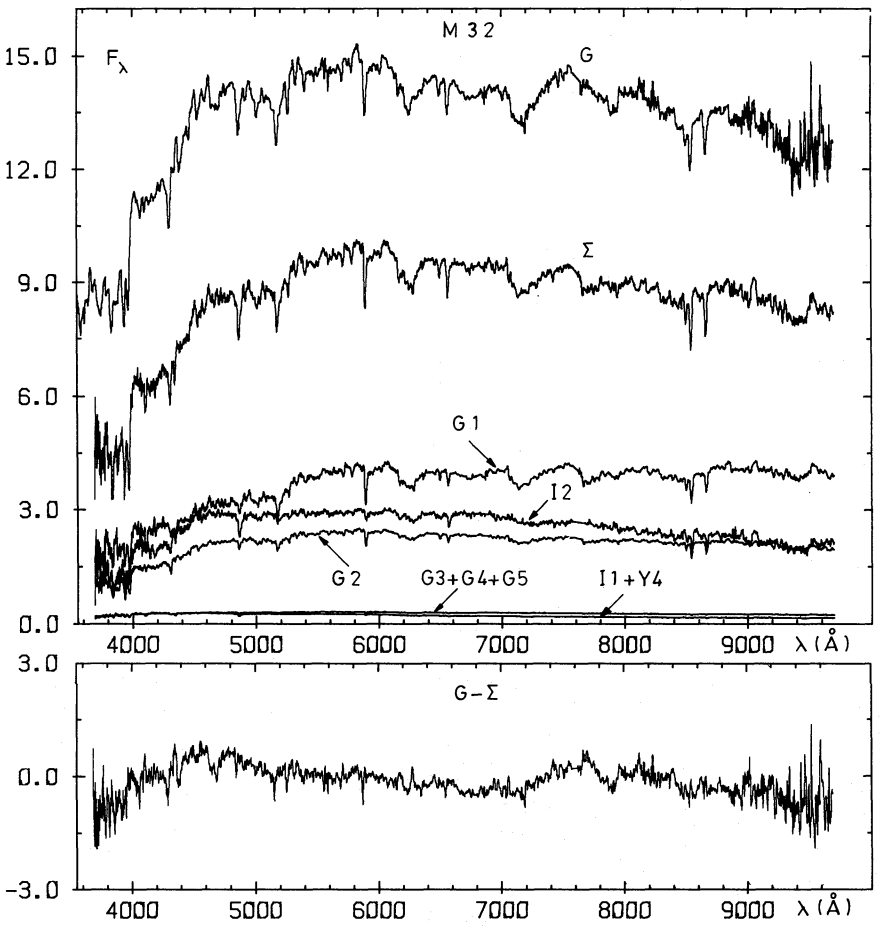

Fig. 4. Visualization of the grid synthesis solution for path A[0.0], for M 32 (∑) using the available star cluster spectral groups (Gi, Ii, Yi). For the age and metallicity values of these groups see Table 7. The real galaxy spectrum is reddening corrected: foreground $E(B-V)_G = 0.08$ and internal $E(B-V)_i = 0.05$. For clarity the observed spectrum G has been shifted along the vertical axis

Table 6. Same as Table 2, for the nucleus in NGC 205. (a) the whole-plane solution; (b) the path solution of type *A*, up to $[Z/Z_\odot] = -0.5$, labelled *A*[−0.5]; (c) the path solution of type *B*, up to solar metallicity, labelled *B*[0.0]

RH II	E7	5 E7	E8	5 E8	E9	5 E9	> E10	Age $[Z/Z_\odot]$
Table 6a								
0.4	15.9	0.6	9.4	0.4	0.4	0.4	2.6	+0.6
	0.5	0.4	0.7	0.9	0.6	0.4	0.6	+0.3
	0.4	0.6	0.4	1.5	0.9	0.7	0.9	0.0
	2.1	1.3	11.9	29.6	1.9	3.0	1.3	−0.5
					2.8	1.3	1.3	−1.0
						1.3	1.3	−1.5
							0.9	−2.0
Acceptable solutions: 158; $\chi^2 = 0.649$								
Table 6b								
0.4								+0.6
								+0.3
								0.0
	13.4	4.2	22.0	29.9	5.5	15.1	4.1	−0.5
							3.8	−1.0
							1.1	−1.5
							0.5	−2.0
Acceptable solutions: 55; $\chi^2 = 0.796$								
Table 6c								
1.0								+0.6
								+0.3
	9.5	0.2	41.5	7.6	3.3	6.6		0.0
							10.9	−0.5
							10.6	−1.0
							7.1	−1.5
							1.9	−2.0
Acceptable solutions: 17; $\chi^2 = 0.998$								

Test

Features	Observed W_λ (Å)	Window (Å)	Residue (Å)		
			a	b	c
Ca II K	5.3	2.5	−0.3	−0.4	−0.4
CN 4216	1.3	3.0	−1.4	−1.1	−2.0
CH G band	3.8	1.5	1.3	1.0	1.1
Mg I + MgH	3.1	1.8	−0.2	0.1	−0.2
Ca II 8542	5.7	2.0	0.6	1.3	1.0
Ca II 8662	5.5	2.0	0.8	1.4	1.1
Hδ	8.4	2.5	−0.4	−0.4	0.0
Hγ	7.7	2.0	0.4	0.3	0.0
Hβ	6.8	1.5	0.3	0.3	0.6

they contain are from the LMC and the Galactic disc (young groups Y1 to Y4 and intermediate age groups I1 and I2). The Galactic globular cluster groups G2 to G5 have an average metallicity $[Z/Z_\odot]$ ranging from −0.4 to −2.0. The strong-lined group G1, with globular clusters like NGC 6528, is not included in the synthesis being too metallic with respect to NGC 205 as shown by the grid synthesis (Table 6). For the very young components, we use in the calculation a continuum derived from observed HII regions affected by internal reddening: it is free of emission lines and acts as a metallicity line diluter in the synthesis, especially in the blue range. The Hα region (6520–6600 Å) is excluded for the calculation, owing to the possible emission

contamination. We have also left out the regions where correction residuals occur at earth atmosphere molecular bands (6830–6940 Å; 7550–7620 Å and 9280–9700 Å).

The flux contributions of the eleven base components and the internal reddening $E(B-V)_i$ were optimized through a routine linked to the MINOS system, that minimizes the differences between the observed spectrum of NGC 205 (corrected for the foreground reddening $E(B-V)_G = 0.04$) and the synthetic one. This synthesis was meant to be a refinement of the grid calculations along paths $A[-0.5]$ and $B[0.0]$. So the component contributions were allowed to vary between their corresponding flux fractions in Tables 6b and 6c. The results are shown in Table 7. An internal reddening $E(B-V)_i = 0.11$ comes out which is not unexpected because dust patches occur in the central regions of NGC 205 (Hodge, 1973). This solution resembles more that corresponding to path $A[-0.5]$ than to $B[0.0]$.

The visualization of the solution from Table 7 in terms of star-cluster components is displayed in Fig. 5. We conclude that the dominant population is young, in the range 10^8–$5\,10^8$ yr. The old components in the range $-0.5 \geq [Z/Z_\odot] \geq -1.0$ and the intermediate age components contribute $\approx 20\%$ each to the optical flux. The maximum metallicity attained in the stellar population of this galaxy is $[Z/Z_\odot] \approx -0.5$ or slightly above this value, but certainly not solar.

Star formation histories can be derived through the present integrated light-matching method (Bica et al., 1988). This may

Table 7. Synthesis of NGC 205 using directly the spectra of star cluster groups as a base

Group	Age (yr)	$[Z/Z_\odot]$	% 5870 Å
H II	$<5\,10^6$	0.0 to −0.5	0.4
Y1	10^7	−0.3	9.5
Y2	$5\,10^7$	−0.2 to −0.6	0.2
Y3	10^8	+0.1 to −1.0	22.0
Y4	$5\,10^8$	−1.1	24.2
I1	10^9	0.0	5.5
I2	$5\,10^9$	−0.6 to −1.0	15.1
G1	$>10^{10}$	+0.2 to 0.0	0.0
G2	$>10^{10}$	−0.4	10.9
G3	$>10^{10}$	−1.0	10.6
G4	$>10^{10}$	−1.5	1.1
G5	$>10^{10}$	−2.0	0.5

Notes: Columns: (1) identification of the star cluster group according to Bica (1988); (2) and (3) mean age and metallicity of the clusters in each group; (4) and (5) results of the synthesis expressed in terms of flux fractions at 5870 Å. The internal reddening being a free parameter in the optimization, resulted as $E(B-V)_i = 0.11$

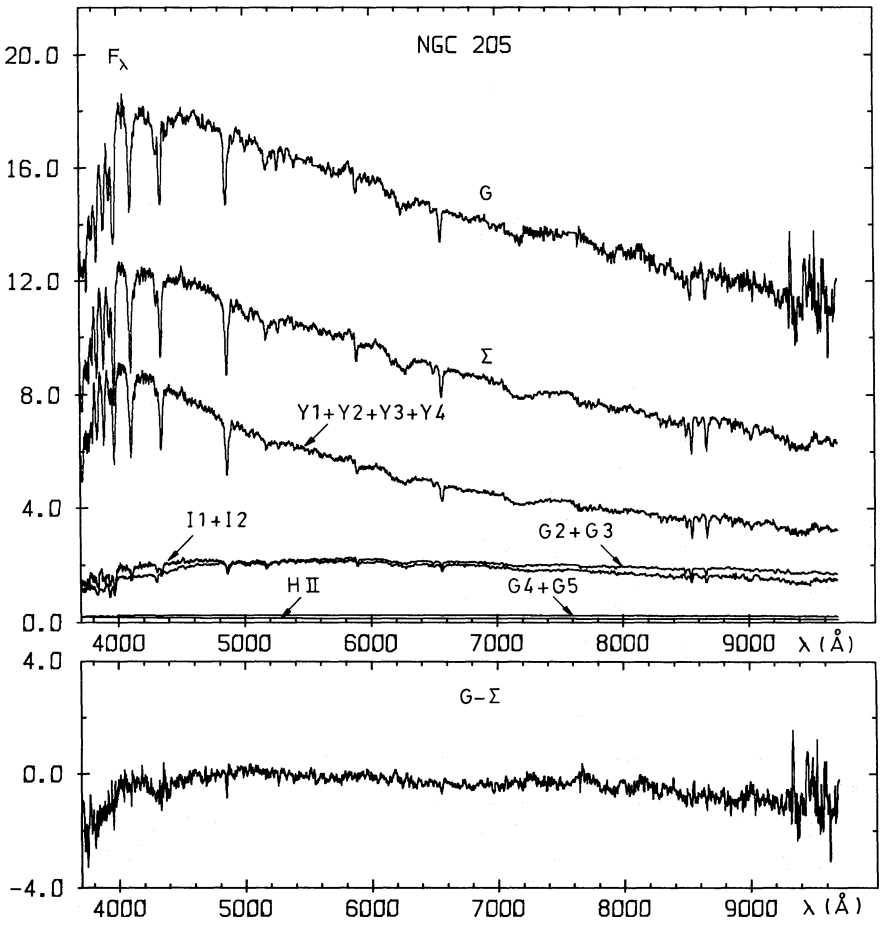

Fig. 5. Visualization of the point to point spectral synthesis ($\sum$) for NGC 205 (model from Table 7). The real galaxy spectrum has been corrected for the foreground reddening $E(B-V)_G = 0.04$ and an internal one $E(B-V)_i = 0.11$. For clarity the observed spectrum G has been shifted along the vertical axis

be of great help to calibrate the relative numbers of luminous stars in colour-magnitude diagrams of nearby galaxies in terms of their age distribution, in view of studying space telescope colour-magnitude diagrams beyond.

7. Search for faint emission lines

The stellar-subtracted spectra (residuals) are used to search for emission lines. In general, the strongest emission lines in the optical region are Hα, [NII] 6584 Å and [SII] 6717.31 Å for galaxies with low luminosity emission components (e.g. Keel, 1983). We point out that in the visualization of the grid synthesis, group G1 which contains strong-lined globular clusters like NGC 6528 (Bica, 1988), represents well the old metal rich component for populations as strong-lined as the inner bulge of M 31 (Fig. 3). However, as already found for even more strong-lined early type galaxies (E1 group in Bica, 1988), significant metallic residuals remain. This is also the case for the semistellar nucleus of M 31. Nevertheless we can temporarily use G1 to represent the old metal-rich component of the SSN, as metallic features are not very strong in the 6500–6800 Å region. The population-subtracted spectra are shown in Fig. 6a for the M 31 SSN and the bulge. Weak [NII] and [SII] lines and possibly Hα are detected in the bulge. Although there is some evidence of Hα in the SSN, this result is marginal because the emission line at low levels is particularly sensitive to errors in the absorption component. The detection of some ionized gas in the bulge and little or even no emission in the SSN confirms the results from previous observations (Rubin and Ford, 1986 and references therein).

We have displayed in Fig. 6b the population-subtracted spectra for M 32 and NGC 205. In both objects residuals of Hα absorption are conspicuous. M 32 does not show any emission while in NGC 205 there is marginal evidence for [NII] and [SII] lines. However, their level is so weak that current star formation must be essentially absent, indicating that the burst of star formation seen as a blue stellar component (Fig. 5) must have become inoperative.

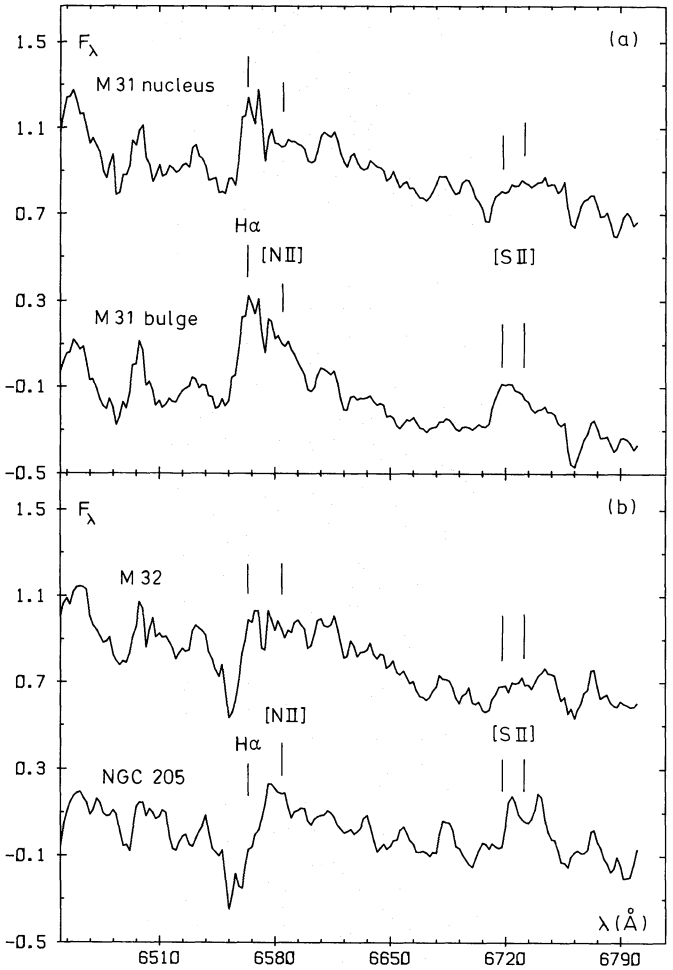

Fig. 6. Search for emission lines in the (observed minus synthetic) spectra. The vertical scale corresponds to $F_\lambda = 10$ at 5870 Å for the continuum in the original spectra. The expected positions of emission lines are indicated. *a* M 31 semistellar nucleus and bulge; *b* M 32 and NGC 205

8. Concluding remarks

To summarize this study, let us point out that we have performed new population syntheses of the nuclear regions in M 31 and of its dwarf elliptical companions M 32 and NGC 205, using a star cluster base exclusively. This alternative method with respect to those making use of stellar libraries, does not require any direct assumption about the IMF and the stellar evolution. It provides the visible flux fractions from different age and metallicity components as well as the overall chemical evolution in the object. It has given insight into some questions not yet solved by the traditional methods using stellar libraries such as the intermediate age content for M 32.

The ranking of maximum metallicity attained in the stellar population is as follows: M 31 SSN, M 31 bulge, M 32 and NGC 205, which are respectively $[Z/Z_\odot] = 0.6$, 0.3, 0.0 and −0.5. In all cases our results indicate a metallicity dispersion within the old age bin. The dominant stellar component is of a different age among these systems. The M 31 SSN and bulge are dominated by the old components with an additional 10–20% flux contribution from intermediate ages and a negligible flux fraction from young components in the visible and near-infrared ranges. In M 32, the intermediate age component is more important than in the nucleus of M 31, but it is definitely not dominant (≈30% in flux); the old components of moderate metallicity are dominant while the young component is negligible. The visible light from NGC 205, on the other hand is dominated by young components in the range 10^8–$5\,10^8$ yr. The intermediate age and the old age components each contribute ≈20% of the optical flux.

The star formation histories derived through the present method may be important for the calibration of the relative numbers of luminous stars in colour-magnitude diagrams of nearby galaxies, in terms of age proportions of stellar populations: a step toward the analysis of space telescope colour-magnitude diagrams beyond.

We are also aware of possible future improvements on this method: (i) the analysis of young and intermediate age populations will greatly benefit from the inclusion of data points shortward of 3800 Å and so to do we are extending the star cluster and galaxy data bases over the 1200–3800 Å range, (ii) the star cluster base is being implemented with M 31 metal-rich globular clusters in order to better span the age-metallicity plane, and (iii) the impact of the second parameter problem in globular clusters on the present synthesis method is to be investigated.

Acknowledgements. We thank the staff at the Haute Provence Observatory for assistance during the observations. We are gratefully indebted to R. O'Connell for interesting comments on an earlier version of this work. A.S. and E.B. acknowledge research fellowship from the brazilian institution CNPq. E.B. is indebted to Paris Observatory for a temporary assistant position.

References

Alloin, D., Bica, E.: 1989, *Astron. Astrophys.* **217**, 57
Arimoto, N., Yoshii, Y.: 1987, *Astron. Astrophys.* **173**, 23
Bica, E.: 1988, *Astron. Astrophys.* **195**, 76
Bica, E., Alloin, D.: 1986a, *Astron. Astrophys.* **162**, 21
Bica, E., Alloin, D.: 1986b, *Astron. Astrophys. Suppl. Ser.* **66**, 171
Bica, E., Alloin, D.: 1987a, *Astron. Astrophys.* **186**, 49
Bica, E., Alloin, D.: 1987b, *Astron. Astrophys. Suppl. Ser.* **70**, 281
Bica, E., Alloin, D.: 1988a, in *Towards understanding galaxies at large redshifts*, eds. R. Kron and A. Renzini, Kluwer London, New York, p. 77
Bica, E., Alloin, D.: 1988b, *Astron. Astrophys.* **192**, 98
Bica, E., Arimoto, N., Alloin, D.: 1988, *Astron. Astrophys.* **202**, 8
Burstein, D., Heiles, C.: 1984, *Astrophys. J. Suppl. Ser.* **54**, 33
Cohen, J.G.: 1979, *Astrophys. J.* **228**, 405
Faber, S.M.: 1972, *Astron. Astrophys.* **20**, 361
Hodge, P.W.: 1973, *Astrophys. J.* **182**, 671
Gallagher, J.S., Mould, J.R.: 1981, *Astrophys. J.* **244**, L3
Keel, W.C.: 1983, *Astrophys. J.* **269**, 466
Murtagh, B.A., Saunders, M.A.: 1987, *MINOS 5.1 User's Guide*, Technical Report SOL 83-20R, Stanford University, California
O'Connell, R.W.: 1980, *Astrophys. J.* **236**, 430
O'Connell, R.W.: 1986, in *Stellar Populations*, eds. C. Norman, A. Renzini, M. Tosi, Cambridge University Press, Cambridge p. 167
Oke, J.B.: 1974, *Astrophys. J. Suppl. Ser.* **27**, 21
Richer, H.B., Crabtree, D.R., Pritchet, C.J.: 1984, *Astrophys. J.* **287**, 138
Rubin, V.C., Ford, W.K. Jr.: 1986, *Astrophys. J.* **305**, L35
Sandage, A., Tammann, G.: 1981, *A Revised Shapley-Ames Catalogue of Bright Galaxies*, Carnegie Institution of Washington
Schmidt, A.A., Bica, E., Dottori, H.: 1989, Monthly Notices Roy. Astron. Soc. **238**, 925
Spinrad, H., Taylor, B.J.: 1971, *Astrophys. J. Suppl. Ser.* **22**, 445
Stone, R.P.: 1977, *Astrophys. J.* **218**, 767
Welch, G.: 1982, *Astrophys. J.* **259**, 77
Williams, T.B.: 1976, *Astrophys. J.* **209**, 716